DNS ANALYSIS OF SHOCK WAVE / TURBULENT BOUNDARY LAYER INTERACTION AT $M = 2.25$

Sergio Pirozzoli & Francesco Grasso
Dipartimento di Meccanica e Aeronautica,
Universitá di Roma 'La Sapienza'
Via Eudossiana 18, 00184 Roma, Italy
s.pirozzoli@dma.ing.uniroma1.it

Thomas B. Gatski
Computational AeroSciences Branch,
NASA Langley Research Center
Hampton, Virginia 23681-2199, USA
t.b.gatski@larc.nasa.gov

ABSTRACT

In this study the interaction of a supersonic flat plate boundary layer flow with an impinging shock (at $M_\infty = 2.25$ and $Re_\theta \approx 4000$, and shock angle $\beta = 32.7°$) is analyzed by means of a direct numerical simulation. The results show that under such conditions, the flow field dynamics upstream of the impinging shock closely resembles the incompressible pattern; however, in the interaction zone the flow undergoes separation due to the adverse pressure gradient, and the recovery of the universal behavior occurs on a length scale of $O(10\delta_0)$, where δ_0 is the boundary layer thickness in the absence of the interaction. The simulations also clearly suggest severe flapping motion of the reflected shock past the interaction zone, with the generation of sound waves. The results also indicate that the localized turbulence amplification is mainly related to the formation of large vortical structures associated with boundary layer separation.

INTRODUCTION

The physical phenomena associated with unsteady shock wave / boundary layer interaction (SWBLI) are of extreme relevance for aerospace applications, since they can degrade the performance efficiency of aircraft, as well as lead to structural fatigue. SWBLI also takes place in supersonic air intakes and reduces their efficiency when separation becomes strongly unsteady. In addition, the interaction of turbulent eddies with shock waves and the unsteady shedding of vortices downstream of the interaction are known to be a major source of broadband noise. The simulation of such off-design (non-similar and non-equilibrium) phenomena is beyond the capabilities of existing turbulence models and is a challenging task for numerical algorithms.

In the incompressible regime, Na and Moin (1998) have analyzed the separated turbulent boundary layer over a flat plate by means of direct numerical simulations. In their study, a closed separation bubble was caused by an adverse-to-favourable pressure gradient. Under those conditions, large turbulent structures formed near the separation point, and were responsible for turbulent fluctuation amplification away from the wall.

Adams (2000) investigated the turbulent boundary layer along a compression ramp at a free-stream Mach number of $M = 3$ and Reynolds number (based on the momentum thickness) of $Re_\theta = 1685$ by means of a quasi-spatial direct numerical simulation. Under such conditions, a small area of separated flow developed in proximity to the flat plate / ramp juncture with significant shock oscillation and amplification of both normal and tangential Reynolds stresses.

Garnier et al. (2002) analyzed the impingement of an oblique shock wave upon a turbulent boundary layer in the presence of a small separation by means of large eddy simulation (LES), and found good agreement between the computed mean global quantities, such as skin friction and displacement thickness, and experimental results.

The scope of the present DNS study is two fold: i) characterize the unsteady nature of the interaction; and ii) identify and quantify the turbulence amplification mechanisms occurring in the SWBLI.

NUMERICAL METHODOLOGY

The numerical calculation performed in this study is a direct numerical simulation (DNS) of a spatially developing, supersonic turbulent boundary layer interacting with an oblique shock wave. This avoids the limitations of previous quasi-spatial DNS studies performed by early investigators both in the incompressible (Na and Moin, 1998) and in the compressible (e.g. Adams, 2000 and Garnier et al., 2002) regimes. No "slow growth" nor "extended temporal" simplifying assumptions are made here, and the full process of transition and boundary-layer growth is accounted for; thus minimizing any uncertainty on artificial conditions that may be imposed on the flow.

A sketch of the computational domain used here is shown in Fig. 1. An oblique shock wave, whose pressure ratio is $p_1/p_0 \approx 1.6$ is made to impinge on a turbulent supersonic boundary layer developing on a flat plate at $M = 2.25$, $\mathrm{R}e/in = 635000$. The nominal (inviscid) impingement point is at $x \approx 8.66$, where x is measured in units from the leading edge of the flat plate. At that station the (nominal) Reynolds

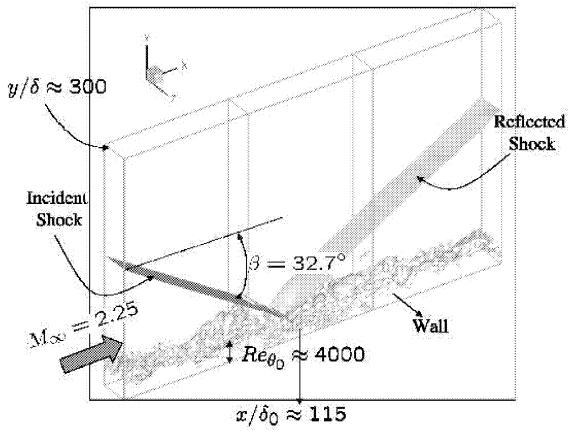

Figure 1: Sketch of the computational domain for DNS of shock wave / turbulent boundary layer interaction.

number based on the momentum thickness is $Re_\theta \approx 4000$. The numerical algorithm solves the full three-dimensional, Navier-Stokes equations in conservation form and relies on a conservative seventh-order finite difference weighted-ENO scheme for the Eulerian fluxes, a fourth order compact-difference scheme to discretize the viscous fluxes, and a fourth-order explicit Runge Kutta time integration algorithm (Pirozzoli et al., 2004). In order to induce laminar-to-turbulent transition, a laminar compressible boundary layer profile is enforced at the inlet (taken at $x = 4$), and a region of blowing and suction between $x = 4.5$ and $x = 5$, (in this region the normal velocity component is nonzero and is introduced to initiate boundary layer instabilities. No-slip, adiabatic boundary conditions are enforced at the bottom wall, extrapolation is used at the outlet boundary together with a buffer zone technique, and non-reflecting boundary conditions are enforced at the upper boundary so as to minimize spurious reflection of disturbances back into the computational domain; finally, periodic boundary conditions are used in the cross-stream direction to exploit homogeneity.

A similar calculation has been carried out previously in the absence of the interaction and the results are reported in Pirozzoli et al. (2004), where the details of the discretization scheme are also provided. In the present study the results of the no-shock case are exploited to initialize the flow field, and the shock is artificially generated by enforcing discontinuous conditions at the inlet boundary that satisfy the Rankine-Hugoniot jump conditions. The flow field is left free to evolve until it reaches a statistically steady state, and then statistical samples are collected at time intervals of $\Delta t \approx 0.1\theta/u_\infty$, until convergence is observed for the lower (up to third) order statistical quantities.

For the no-shock case, a thorough grid sensitivity analysis (Pirozzoli et al., 2004) indicated that a grid spacing of the order of $\Delta x^+ = 15$, $\Delta y_w^+ = 1$, and $\Delta z^+ = 6.5$ is needed in order to achieve a grid independent solution; in addition, the study also showed that a domain with of $L_z^+ \approx 1600$ is sufficient to guarantee that the two-point spanwise correlations of all flow variables drop to zero at the tails of the correlation curve. The same grid resolution (in wall units) is used in the present simulations, although more points are clustered in the wall-normal direction in order to have about 70 points in the interaction region. The selected computational grid includes $2650 \times 111 \times 255$ grid nodes.

RESULTS

Although it is not possible in the space here to fully present the extensive array of results from such a simulation, it is possible to highlight some of the key dynamic features of the flow field. This section is subdivided into three sub-sections that discuss the mean and instantaneous thermodynamic properties of the flow, the effect on the turbulence through the velocity second-moments, the mean velocity filed, and finally some comparison with experiments.

Instantaneous Structure and Mean Properties

The instantaneous flow field is best represented in terms of the density field, which is interpreted for this purpose as a passive scalar. The computed instantaneous and average density fields are depicted in Fig. 2 in terms of iso-contour lines in the $x - y$ plane. (For this purpose note that the average fields for all quantities have been obtained by averaging over time and over the direction of homogeneity, z). The

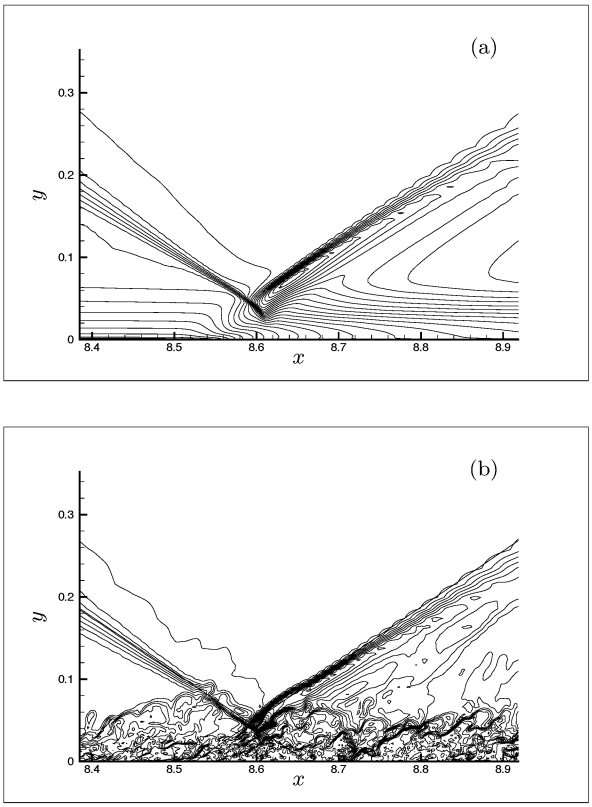

Figure 2: Mean (a) and instantaneous (b) density field in $x-y$ plane in proximity of the interaction zone. 32 contour levels, $0.55 \leq \rho \leq 2.2$.

averaged density field depicts the existence of a very simple flow pattern where the incident shock bends toward the wall while entering the boundary layer, and the reflected shock originates well upstream of the nominal impingement point due to a typical viscous interaction mechanism. In addition, a small separation bubble is observed near the wall between

$8.54 \leq x \leq 8.62$ (which is better exemplified from an analysis of the mean velocity field not shown here for brevity). On the other hand, the instantaneous density field, shown in Fig. 2b, reveals the existence of complex organized motions in the outer layer, that are characterized by the occurrence of turbulent bulges that exhibit a highly intermittent character and that are inclined at an acute angle with respect to the wall. As also observed experimentally both in subsonic and supersonic turbulent boundary layers (Smits and Dussauge, 1996), the figure clearly indicates that these structures are separated from the surrounding essentially irrotational fluid by sharp interfaces having a three-dimensional character. This scenario is consistent with the results of the simulations performed in the absence of the impinging shock (Pirozzoli et al., 2004); however, note that in the presence of SWBLI the interfaces separating rotational and irrotational fluid become sharper past the interaction. The analysis of the time evolution of the flow field also indicates intense flapping motion of the reflected shock, which is distorted due to the interaction with the large vortical structures associated with the incoming turbulent boundary layer. The analysis of the flow animations clearly indicates branching of the reflected shock and propagation of acoustic waves emanating from the interaction zone (which the reader may also infer from inspection of Fig. 2b).

The average and instantaneous pressure field in the interaction zone are depicted in Fig. 3, which consistent with the density visualization, indicates severe unsteady motion of the reflected shock. In addition, Fig. 3 also indicates the generation of large vortical structures that are detectable in the figure as cores of low pressure. Such structures are generated close to the instantaneous separation point, are lifted away from the wall, and interact with the incident shock. These structures, which are a major cause of large scale unsteadiness, propagate downstream of the interaction zone undergoing a slow decay.

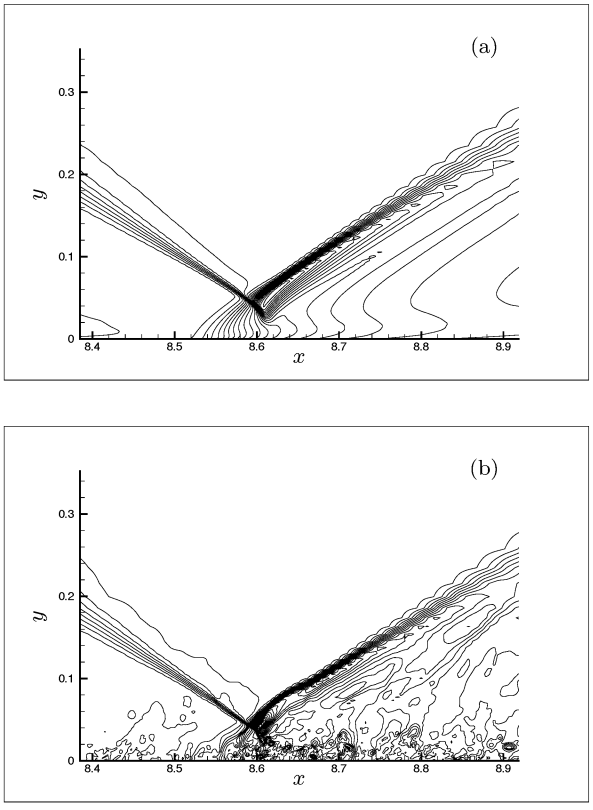

Figure 3: Mean (a) and instantaneous (b) pressure field in $x-y$ plane in proximity of the interaction zone. 40 contour levels, $0.95 \leq p \leq 3.15$.

Analysis of Turbulence properties

The distributions of the specific turbulent kinetic energy ($k = \widetilde{u_i'' u_i''}/2$) and the specific turbulent shear stress ($\tau_{xy} = -\widetilde{u'' v''}$) are shown in Figs. 4 and 5, respectively. The figures indicate that most of the turbulence activity caused by SWBLI is associated with the large vortical structures seen in Fig. 3b. In particular, the specific turbulent kinetic energy attains an absolute maximum close to the mean separation point, and exhibits a (decreasing) local maximum in the streamwise direction well away from the wall, corresponding to the zone where coherent structures propagate. On the other hand, the specific turbulent shear stress attains its maximum value downstream of the interaction zone, and its production appears to be also strongly correlated with the existence of persistent coherent structures. The apparent mismatch of peak specific kinetic energy and shear stress levels suggest that the energy production mechanism in some regions may be due mainly to compressibility effects rather than the usual shear stress production mechanism. Finally note that the shear stress levels (and to a lesser extent energy levels) are augmented along the direction of the reflected shock.

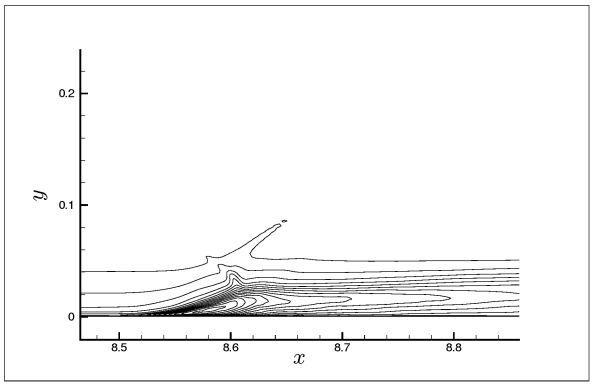

Figure 4: Distribution of specific turbulent kinetic energy ($k = \widetilde{u_i'' u_i''}/2$) in $x-y$ plane in proximity of the interaction zone. 16 contour levels, $0 \leq k \leq 0.36$.

Behavior of mean velocity profiles

In Fig. 6, the distribution of the average streamwise velocity component ($\overline{u}$) at several streamwise stations are shown: the first station corresponds to a point located well upstream of the interaction; the second one corresponds to a point inside the interaction zone before separation; the third one is located downstream of the interaction, but in the vicinity of it; and a fourth point that is further downstream. Note that, for the purpose of assessing the existence of a universal velocity distribution (as well as deviations from it) the Van Driest transformed average velocity ($\overline{u}_c$) has been considered (e.g.,

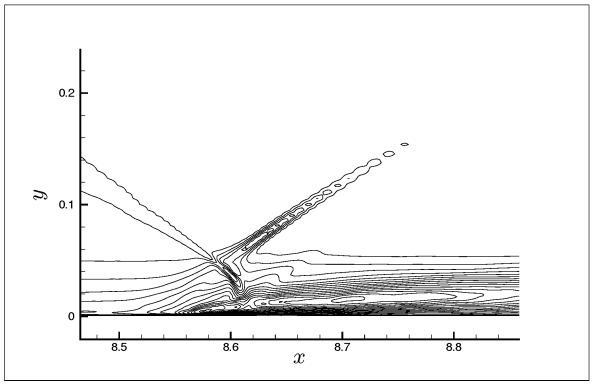

Figure 5: Distribution of specific turbulent shear stress ($\tau_{xy} = -\widetilde{u''v''}$) in $x-y$ plane in proximity of the interaction zone. 16 contour levels, $0 \le k \le 0.38$.

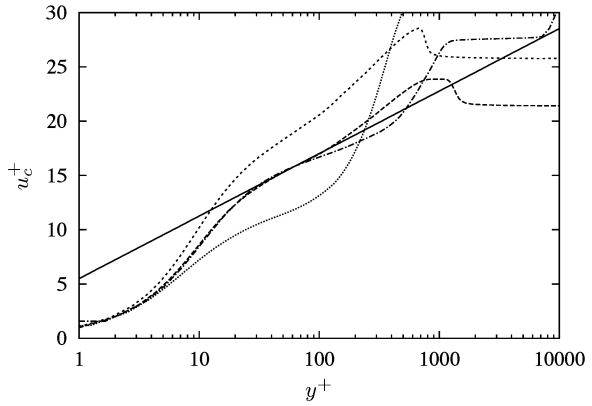

Figure 6: Distribution of Van Driest transformed mean streamwise velocity at several streamwise stations. ——, $u^+ = 5.5 + 2.5 \log y^+$; – – – –, $x = 8.44$; - - - - -, $x = 8.52$; · · · · · · ·, $x = 8.76$; - · - · -, $x = 9.50$.

White, 1974).

$$\overline{u}_c = \int_0^{\overline{u}} \left(\frac{\overline{\rho}}{\overline{\rho}_w} \right)^{1/2} \mathrm{d}\overline{u} \ .$$

For an equilibrium, zero pressure gradient, the turbulent boundary layer exhibits a multi-layer, universal structure. In particular, for the average velocity in the overlap layer it satisfies a log-law of the form

$$u_c^+ = \frac{1}{\kappa} \log y^+ + C,$$

where $\kappa \approx 0.4$, $C \approx 5.5$, and 5

$$u_c^+ = \frac{\overline{u}_c}{u_\tau}, \quad y^+ = \frac{y u_\tau}{\nu_w}, \quad u_\tau = \left(\frac{\tau_w}{\rho_w} \right)^{1/2} \ .$$

Figure 6 indicates that a log-layer indeed exists upstream of the interaction (for $30 \le y^+ \le 100$); however, this equilibrium layer is lost across the interaction zone (i.e. stations 2 and 3), with large deviations for stations upstream of the separation point and downstream of the reattachment. However, the flow exhibits a tendency to recover a universal behavior on a spatial scale of $O(10\delta_0)$, (δ_0 is the boundary thickness in the absence of the interaction). at the fourth and final station shown, a log-layer is exhibited in the range (approximately) $30 \le y^+ \le 60$.

Comparison with experiments

In order to compare the present results with existing experimental data, the experiments of Deleuze (1995) and Laurent (1996) have been selected. Their conditions are sufficiently close to the present ones ($M = 2.28$ and $Re_\theta \approx 5000$) to allow for qualitative comparison. In order to help validate the present simulation results, Fig. 7 shows the distribution of the computed nondimensional wall pressure and average skin friction coefficient as a function of the nondimensional streamwise coordinate $\xi = (x - x_0)/(x_r - x_s)$, where x_0 is the nominal impingement point, and x_s and x_r are, respectively, the average location of separation and reattachment. The distribution of

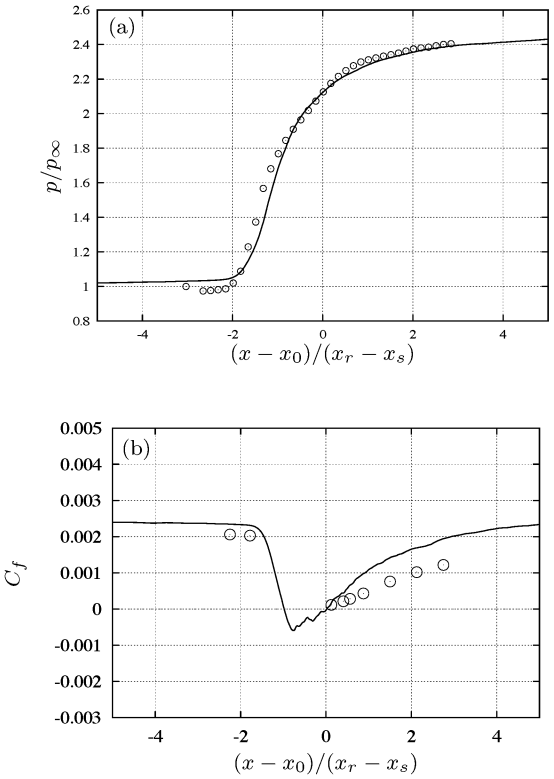

Figure 7: Validation study: comparison of the DNS data with experimental measurements (Deleuze, 1995). (a) distribution of (nondimensional) average wall pressure; (b) distribution of the average skin friction coefficient. ——, DNS data; ∘, experimental data.

the wall pressure shows good quantitative agreement between the DNS and experiment, and in particular, it indicates the absence of a significant pressure plateau, which is typical of incipient separation conditions. The distribution of the skin friction coefficient also shows a good overall qualitative agreement; however, significant differences are found in the recovery zone, and in particular the DNS relaxes faster toward equilibrium than the experiment. This may be due to the different structure of the boundary layers upstream of the interaction (different Re_θ values), which yields a $O(20\%)$ difference in the value of the skin friction.

CONCLUSIONS

In this study, the interaction of a supersonic flat plate boundary layer flow with an impinging shock wave has been analyzed by means of a fully spatial direct numerical simulation that relies on the use of a mixed weighted-ENO compact-difference method for the three-dimensional Navier-Stokes equations. The simulations indicate that, under the selected test conditions, the boundary layer undergoes mild separation due to the adverse pressure gradient, and the flow exhibits a strongly unsteady character. In particular, the reflected shock wave exhibits branching and a flapping motion; long-lived coherent vortical structures are periodically generated close to the separation point, and their interaction with the impinging shock is believed to be the main cause of flow unsteadiness. Such structures also are mainly responsible for turbulence amplification past the interaction. The analysis of the average streamwise velocity profiles indicates a loss of universality in the vicinity of the interaction zone, and recovery on a spatial scale of $O(10\delta_0)$ is required for the mean field. Such relaxation effects suggest that flow modification strategies will have a significant effect on the flow for a rather significant spatial distance. Finally, the comparison with experimental results (at somewhat different flow conditions) show good qualitative agreement with both the pressure and skin friction distributions.

REFERENCES

Adams, N. A., 2000, "Direct numerical simulation of the turbulent boundary layer along a compression ramp at $M = 3$ and $Re_\theta = 1685$," *J.* Fluid Mech., Vol. 420, pp. 47–83.

Deleuze, J., 1995, "Structure d'une couche limite soumise à une onde de choc incidente," Thèse de doctorat, Université Aix-Marseille II.

Garnier, E., Sagaut, P., and Deville, M., 2002, "Large eddy simulation of shock/boundary layer interaction," *A*IAA J., Vol. 40, pp. 1935–1944.

Laurent, H., 1996, "Turbulence d'une interaction onde de choc / couche limite sur une paroi adiabatique ou chauffée," Thèse de doctorat, Université Aix-Marseille II.

Na, Y., and Moin, P., 1998, "Direct numerical simulation of a separated turbulent boundary layer," *J.* Fluid Mech., Vol. 374, pp. 379–405.

Pirozzoli, S., Grasso, F., and Gatski, T. B., 2004, "Direct numerical simulation and analysis of a spatially evolving turbulent boundary layer at $M = 2.25$," *P*hys. Fluids, Vol. 16, pp. 530–545.

Smits, A. J., and Dussauge, J. P., 1996, *Turbulent shar layers in supersonic flow*, American Institute of Physics, New York.

White, F. M., 1974, *Viscous fluid flow*, McGraw-Hill, New York.